

## Light Amplification Using Inverted Core/Shell Nanocrystals: Towards Lasing in the Single-Exciton Regime

Sergei A. Ivanov, Jagjit Nanda, Andrei Piryatinski, Marc Achermann, Laurent P. Balet, Iliia V. Bezel, Polina O. Anikeeva, Sergei Tretiak, and Victor I. Klimov\*

Los Alamos National Laboratory, Los Alamos, New Mexico 87545

Received: April 15, 2004; In Final Form: June 3, 2004

Size-controlled spectral tunability and chemical flexibility make semiconductor nanocrystals (NCs) attractive as nanoscale building blocks for color-selectable optical-gain media. The technological potential of NCs as lasing materials is, however, significantly diminished by highly efficient nonradiative Auger recombination of multiexcitons leading to ultrafast decay of optical gain. Here we explore a novel approach to achieve NC lasing in the Auger-recombination-free regime by using type II NC heterostructures that promote spatial separation of electrons and holes. We show that such hetero-NCs can exhibit strong repulsive exciton–exciton interactions that lead to significantly reduced excited-state absorption associated with NCs containing single electron–hole pairs. This effect leads to reduced optical-gain thresholds and can potentially allow lasing in the single-exciton regime, for which Auger recombination is inactive. We use these novel hetero-NCs to demonstrate efficient amplified spontaneous emission (ASE) that is tunable across a “difficult” range of green and blue colors. The ASE in the blue range has never been previously achieved using traditional NCs with type I carrier localization.

Chemically synthesized semiconductor nanocrystals (NCs) are considered to be promising building blocks for novel color-selectable optical-gain media<sup>1,2</sup> because of NC-size-controlled emission colors and potentially low, temperature-insensitive gain thresholds. Tunable optical gain and amplified spontaneous emission (ASE) have recently been demonstrated in the visible and near-IR spectral ranges using CdSe<sup>1–4</sup> and PbSe<sup>5</sup> NCs, respectively. Despite the success of these first experiments, indicating the feasibility of NC lasing, there are still several fundamental problems that hinder applications of NC materials in laser technologies. One such problem is associated with ultrafast optical gain decay induced by nonradiative Auger recombination.<sup>6–8</sup>

In CdSe NCs, optical gain occurs if the average number of electron–hole (e–h) pairs (excitons) per nanoparticle,  $N$ , is greater than 1.<sup>1,2</sup> This requirement indicates that optical gain in these NCs relies on *multiexciton* states (biexciton, triexcitons, etc.), and therefore, its dynamical and spectral properties are strongly affected by exciton–exciton (x–x) interactions.<sup>1–3,5,7–8</sup> In particular, these interactions open a highly efficient *nonradiative* decay channel (picosecond time scale) associated with an Auger-type process, in which the e–h recombination energy is transferred to a third particle (an electron or a hole).<sup>7</sup> Because of rapid shortening of Auger lifetime, with decreasing NC radius,  $R$ , it becomes progressively more difficult to achieve the optical gain and ASE regimes for shorter wavelengths that require the use of NCs of small sizes. For example, although CdSe NCs exhibit strong optical-gain performance in the red to yellow spectral ranges, they do not show efficient ASE in the range of green to blue colors.

Here, we utilize heterostructuring of individual NCs as a means of controlling x–x interactions and enhancing the NC optical-gain performance. This approach allows us to suppress

Auger recombination and simultaneously reduce excited-state absorption arising from singly excited NCs, which makes it possible to demonstrate efficient ASE in the green to blue range of the optical spectrum. Furthermore, we show that the use of appropriately tailored hetero-NCs can, in principle, allow lasing in the *single-exciton regime*, which completely eliminates the problem of Auger recombination.

Core/shell NC heterostructures can show either type I or type II carrier localization, depending on the energy offsets between the core and the shell materials, effective masses, and the relation between the core diameter and the shell thickness. The type I regime corresponds to the situation in which both an electron and a hole are predominantly located in the same part of the heterostructure (in the core or in the shell), while in the type II regime, electrons and holes are spatially separated and occupy different parts of the hetero-NC. Most of the previous studies have concentrated on type I core/shell NCs, in which overcoating with a shell of a wide gap semiconductor is used to improve photoluminescence (PL) quantum efficiencies of the NCs (e.g., refs 9–15). Some work has also been done on inverted type I structures that favor carrier localization in the shell and produce emission with a wavelength tunable by the shell thickness (e.g., refs 15–20). Recently, type II hetero-NCs were studied in the context of producing new emission colors that are not accessible with either core or shell materials alone.<sup>21</sup>

In this work, we study inverted ZnSe/CdSe hetero-NCs in which a core of a wide-gap semiconductor (ZnSe, energy gap  $E_g = 2.74$  eV at 300 K) is surrounded by a shell of a narrower-gap material (CdSe,  $E_g = 1.74$  eV at 300 K). We synthesize these structures via temperature-controlled deposition of CdSe onto ZnSe seed particles in a coordinating solvent (see Supporting Information). The fabricated NCs produce efficient emission (absolute quantum yields up to 60–80%), which is tunable from 430 to 600 nm. The emission line widths are

\* To whom correspondence may be addressed. E-mail: klimov@lanl.gov.

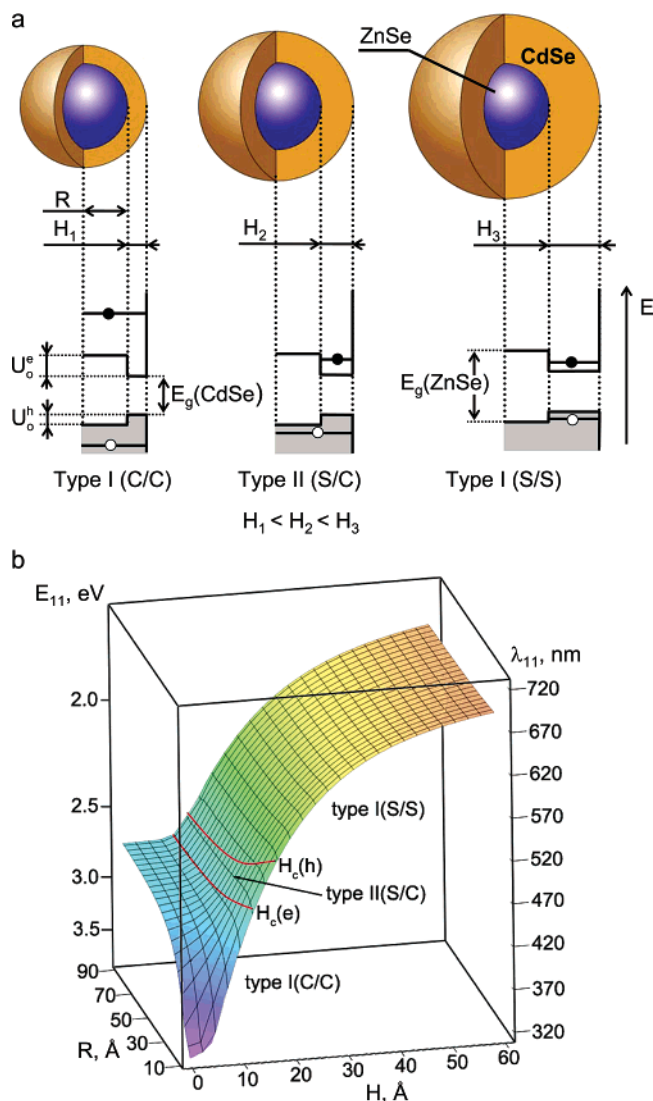


**Figure 1.** (a) Three different localization regimes supported by inverted ZnSe/CdSe hetero-NCs in the case of a fixed core radius and different shell widths. Thin shell (left): Both electron and hole wave functions are delocalized over the entire hetero-NC (type I(C/C) regime). Intermediate shell (middle): The hole wave function is still delocalized over the entire heterostructure, while the electron is confined primarily in the shell (type II(S/C) regime). Thick shell (right): Both the electron and the hole are localized mostly in the shell (type I(S/S) regime). (b) The energy/wavelength of the lowest transition of the hetero-NC plotted as a function of core radius and shell thickness. Two red lines mark the energies corresponding to the transitions between different localization regimes.

from 20 to 40 nm, which is comparable to the PL broadening observed for traditional CdSe NCs, indicating good monodispersity of NCs.

ZnSe and CdSe are characterized by type I energy offsets in the bulk form ( $U_0^e = 0.86$  eV and  $U_0^h = 0.14$  eV, see Figure 1a) that should nominally favor localization of both carriers in CdSe. However, a core/shell ZnSe/CdSe nanostructure can exhibit either type I or type II behavior, depending upon the ZnSe core radius,  $R$ , and the CdSe shell thickness,  $H$ . In particular, for a fixed core radius, one can continuously tune the localization regime from type I to type II and then back to type I by varying  $H$  (Figure 1a). Critical shell widths,  $H_c(e)$  and  $H_c(h)$ , that separate these regimes are determined from the condition  $E_1^{e(h)} = U_0^{e(h)}$ , where  $E_1^{e(h)}$  is the lowest eigenenergy of an electron (a hole) calculated with respect to the bottom of the conduction (valence) band of bulk CdSe. For a shell width  $H < H_c(e)$ , both

an electron and a hole are delocalized over the entire NC (type I(C/C) localization, Figure 1a, left). For  $H_c(e) < H < H_c(h)$ , the electron becomes primarily confined to the shell region, while the hole wave function still remains distributed over the entire hetero-NC. In this regime, however, the hole is found in the core with a much greater probability than in the shell. Therefore, this situation can be described in terms of a charge-separated, spatially indirect exciton (type II(S/C) localization, Figure 1a, middle). As the shell width is increased above  $H_c(h)$ , the hole also becomes primarily localized in the shell, which corresponds to the restoration of type I localization but with both carriers confined to the shell region (type I(S/S) regime, Figure 1a, right).

Figure 1b shows the calculated dependence of the lowest transition energy,  $E_{11}$ , and the corresponding wavelength,  $\lambda_{11}$ , on the core radius and shell thickness. Two red lines mark the energies that correspond to the critical shell widths  $H_c(e)$  and  $H_c(h)$  that separate different localization regimes. In the case of type I(C/C) localization, the energy of the lowest transition is strongly dependent upon both  $R$  and  $H$  (i.e., on the size of the entire hetero-NC), while for the type II(S/C) and type I(S/S) localization,  $E_{11}$  is primarily determined by the width of the shell. The changes in the localization regime, however, do not significantly alter the scaling of the Coulomb interactions that remain approximately inversely proportional to the size of the entire NC, further suggesting that Auger recombination times will scale in proportion to the total volume of the hetero-NCs (independent of the localization regime), as in the case of traditional monocomponent nanoparticles.<sup>7,8</sup> These observations indicate that inverted ZnSe/CdSe structures with a large core radius and a thin shell can significantly reduce Auger recombination rates but still maintain the strong confinement that is required for producing emission in the green to blue range of the spectrum.

To experimentally detect the transitions between different localization regimes, we analyze a series of optical absorption spectra (Figure 2a) recorded for hetero-NCs with the same core size and a varied shell thickness (controlled by reaction time,  $t$ ). For seed ZnSe NCs, the lowest absorption maximum (denoted as 1S) occurs at 354 nm, which corresponds to a seed radius of  $\sim 15$  Å. After the deposition of a CdSe shell has begun, the 1S peak rapidly shifts to 420–430 nm (aliquot 1 in Figure 2a), indicating an increase in the effective volume of the exciton, which, however, remains “spatially direct” (the type I(C/C) localization), as indicated by the presence of a well-defined 1S absorption maximum. A further increase in the shell thickness leads to smearing out of the 1S absorption peak (aliquot 4 in Figure 2a), which is accompanied by a significant increase in the shift between the lowest absorption feature (determined from the analysis of the second derivative of the absorption spectrum) and the PL maximum (Figure 2b). These modifications, however, are not accompanied by an increase in the PL broadening, indicating that they are not due to an increase in sample polydispersity but are rather due to the transition to a type II(S/C) *spatially indirect exciton* that is characterized by reduced oscillator strength. As the shell thickness is further increased, we observe a gradual restoration of the sharp band-edge absorption peak (aliquots 7, 12, and 17 in Figure 2a) indicating a transition to the type I(S/S) localization characterized by the increased e–h overlap. From comparative analysis of PL and the second derivative of absorption spectra (Figure 2b), as well as from the radiative decay dynamics (not shown), we conclude that the transitions between different localization regimes occur at emission wavelengths of  $\sim 460$  nm [I(C/C) to II(S/C)] and  $\sim 510$  nm [II(S/C) to I(S/S)]. In Figure 2b, the type II localization

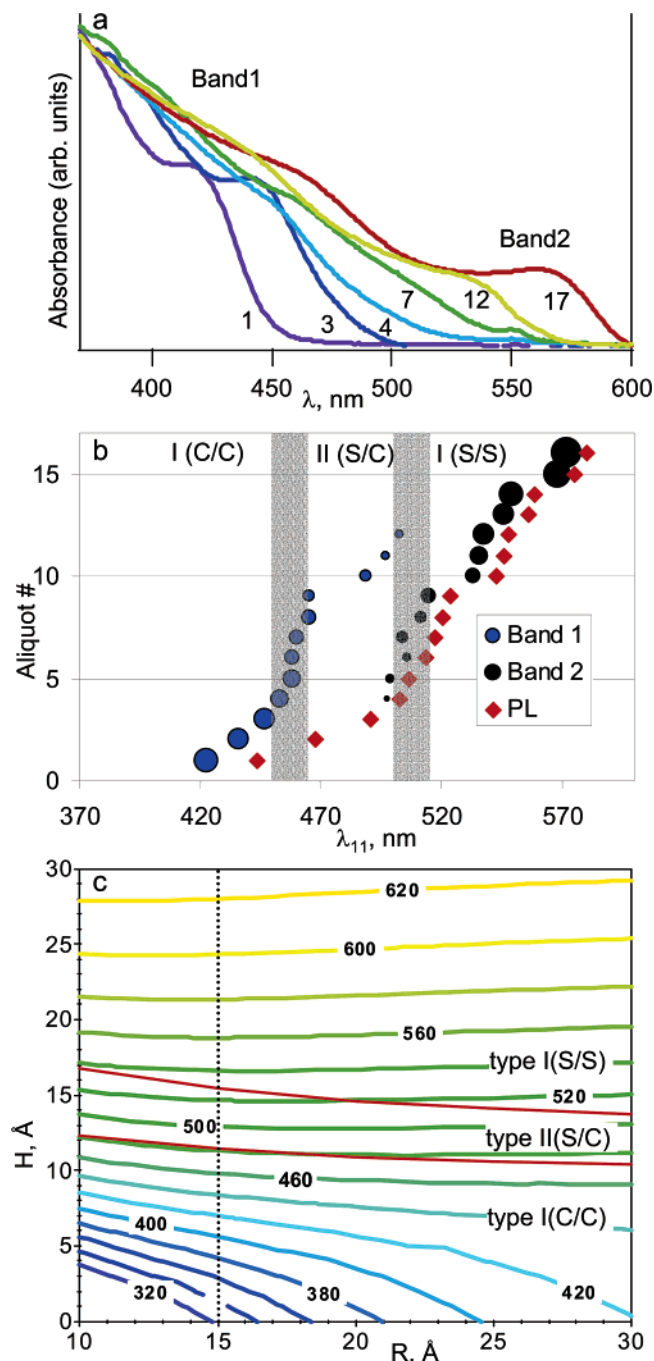


**Figure 2.** (a) Optical absorption spectra of inverted ZnSe/CdSe hetero-NCs with a fixed core radius ( $\sim 15$  Å) and different shell widths. (b) Evolution in the positions of the PL band ( $\blacklozenge$ ) and the minima of the second derivative of absorption spectra ( $\bullet$ ) (these minima mark the absorption peaks) for samples shown in panel a; circle sizes provides an approximate amplitude of the second-derivative minima (this amplitude roughly describes the strength of the corresponding absorption feature). (c) Contour representation of the  $\lambda_{11}(R,H)$  plot using "equal-wavelength" lines. The intersections of the contour lines with the dotted vertical line describe the progression of transition wavelengths realized for a fixed core radius of 15 Å and increasing shell width (approximately corresponds to the situation shown in panels a and b). Two red lines mark the boundaries between three different localization regimes.

approximately corresponds to the range of spectral energies, within which we observe the unusually large shift between the PL band and the first well-pronounced absorption feature. This absorption feature is likely due to a spatially direct transition, which, however, is not the lowest in energy. The actual lowest transition is weak because of its spatially indirect character and,

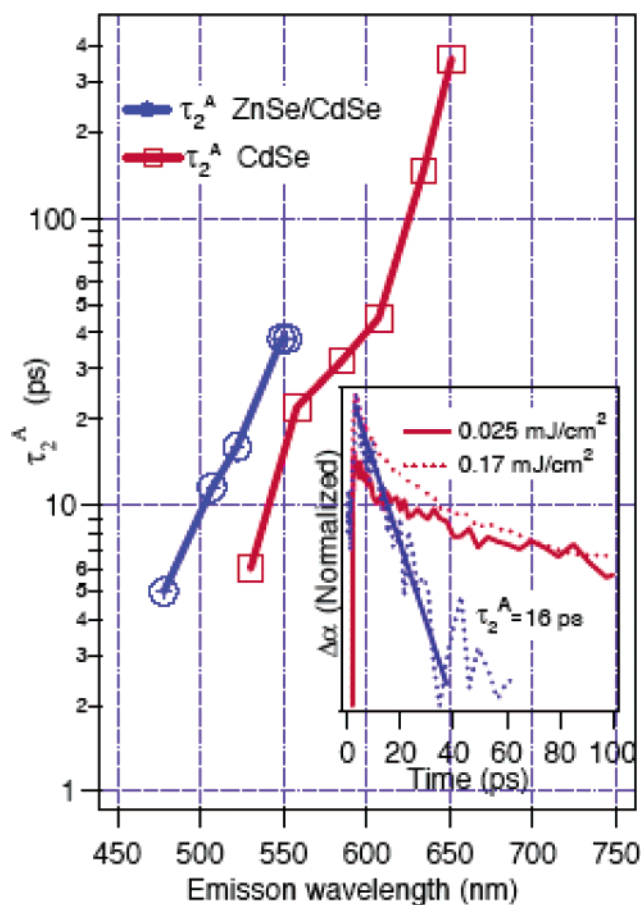


**Figure 3.** The dependence of the biexciton Auger lifetime on the emission wavelength for CdSe ( $\square$ ) and ZnSe/CdSe ( $\circ$ ) NCs. Inset: Population dynamics measured at low (solid line,  $0.025$  mJ/cm $^2$ ) and high (dashed line,  $0.17$  mJ/cm $^2$ ) excitation intensities used to extract the biexciton lifetime of a hetero-NC sample emitting at 522 nm.<sup>6,7</sup>

therefore, is not well pronounced in the absorption spectra. Experimental values for spectral boundaries separating different localization regimes are in good agreement with those predicted by our theoretical model (Figure 2c).

To analyze the effect of different localization regimes on the efficiency of Auger recombination, we measure the Auger lifetime of biexcitons,  $\tau_2^A$ , (Figure 3, inset) using procedures similar to those described in refs 7 and 8. In Figure 3 (main panel), we compare  $\tau_2^A$  plotted as a function of the emission wavelength for ZnSe/CdSe hetero-NCs ( $\circ$ ) and CdSe NCs ( $\square$ ). As expected from the analysis above, heteroparticles provide longer Auger lifetimes when compared to traditional CdSe NCs for PL wavelengths in the green to blue range. For example, for CdSe NCs emitting at 530 nm  $\tau_2^A = 6$  ps, while for ZnSe/CdSe NCs emitting at approximately the same wavelength, this constant is  $\sim 20$  ps, (i.e., 3 times longer).

The ability to suppress the Auger recombination while maintaining strong quantum confinement allows us to significantly extend the short-wavelength range of the ASE regime that is accessible with NCs. The shortest wavelength for which room-temperature light amplification has been obtained using CdSe NCs is  $\sim 580$  nm (yellow color) (Figure 4a, dashed yellow line). By use of ZnSe/CdSe hetero-NCs, we are able to demonstrate room-temperature ASE that is continuously tunable from 565 nm (green) to 523 nm (green-blue) (Figure 4a). The ASE short-wavelength range can further be pushed to 475 nm (cyan-blue color) (main panel and inset in Figure 4a) using liquid

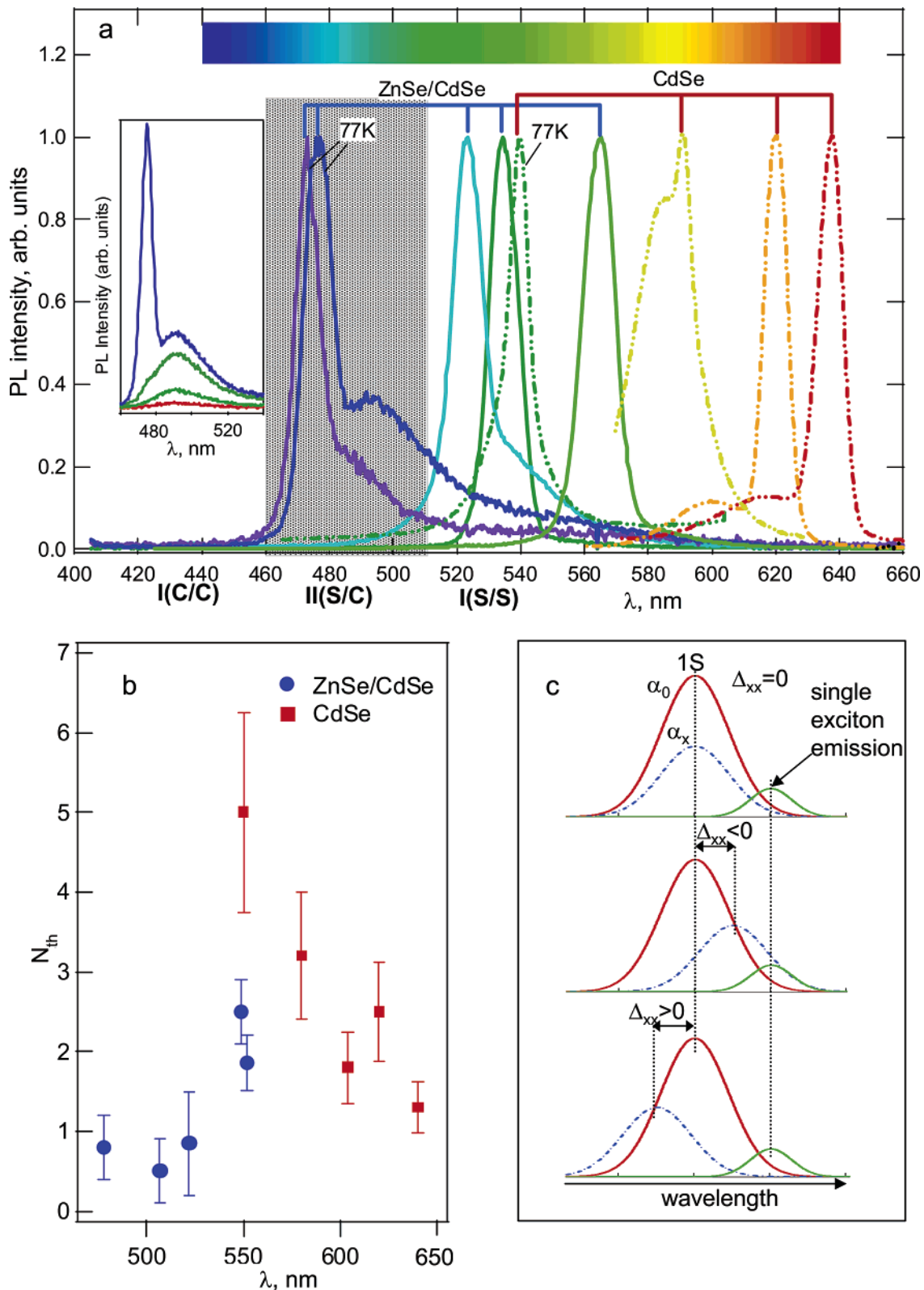


**Figure 4.** (a) ASE, tunable from red to blue using CdSe and ZnSe/CdSe NCs, measured at room temperature and  $T = 77$  K (marked). All samples are excited at 400 nm using frequency-doubled 100-fs pulses from an amplified Ti-sapphire laser. Inset: The development of a sharp ASE peak at 475 nm (blue) in emission spectra of ZnSe/CdSe NCs ( $T = 77$  K) (the pump intensity is ramped from 0.002 to 0.068 mW). The shaded area approximately corresponds to wavelengths for which the type II(S/C) localization is realized. (b) Optical-gain thresholds plotted as a function of emission wavelength for CdSe (■) and ZnSe/CdSe (●) NCs. For both types of samples, thresholds are shown in terms of average NC populations,  $N_{th}$ . (c) The effect of  $x-x$  interactions on the spectral position of excited-state absorption ( $\alpha_x$ ) as compared to the ground-state absorption ( $\alpha_0$ ) and PL spectra. Top (noninteracting excitons,  $\Delta_{xx} = 0$ ): the  $\alpha_x$  spectrum is centered at the same wavelength as the  $\alpha_0$  spectrum. Middle (attractive exciton-exciton interactions,  $\Delta_{xx} < 0$ ): the  $\alpha_x$  spectrum shifts red, which increases excited-state absorption at the gain wavelength. Bottom (repulsive exciton-exciton interactions,  $\Delta_{xx} > 0$ ): the  $\alpha_x$  spectrum shifts blue, which leads to decreased excited-state absorption at the gain wavelength; in this situation optical gain can occur in the single-exciton regime.

nitrogen temperature ( $T = 77$  K). On the other hand, the shortest ASE wavelength obtained with CdSe NCs at 77 K is 540 nm.

For CdSe NCs, realization of the ASE regime for shorter wavelengths becomes progressively more difficult because of the rapid decrease in the Auger recombination time (squares in Figure 3), which leads to a fast growth of the gain threshold (squares in Figure 4b). Interestingly, ZnSe/CdSe hetero-NCs demonstrate the opposite trend in that a decrease in the gain threshold is observed for shorter wavelengths (circles in Figure 4b). This decrease occurs despite more efficient Auger recombination, indicating the existence of competing processes that favor ASE at shorter wavelengths in hetero-NCs.

One effect that can facilitate the achievement of the ASE regime is  $x-x$ -interaction-induced reduction of the excited-state absorption ( $\alpha_x$ ) associated with NCs containing single excitons. Because of the degeneracy of the lowest "emitting" states, singly excited NCs still contribute to the band-edge absorption. However, this excited-state absorption can be spectrally offset with respect to absorption in unexcited NCs due to a transition shift ( $\Delta_{xx}$ ) caused by  $x-x$  interactions.<sup>22</sup> Since optical gain occurs at energies below the lowest absorption maximum, excited-state absorption increases in the case of the red shift ( $\Delta_{xx} < 0$ ; attractive  $x-x$  interaction) and decreases in the opposite case ( $\Delta_{xx} > 0$ ; repulsive  $x-x$  interaction) (Figure 4c). As indicated by both transient absorption<sup>22,23</sup> and PL<sup>24</sup> studies in CdSe NCs,  $\Delta_{xx}$  is negative. However, the sign of the  $x-x$  interaction can change in the case of type II localization, for which charges of the same sign (two electrons or two holes) are forced to co-occupy the same part of the heterostructure. Such co-occupation increases the repulsive component of the Coulomb interaction energy and can lead to the situation for which  $\Delta_{xx} > 0$ , as has been previously observed, e.g., in type II double quantum well structures.<sup>25</sup> The possibility of  $x-x$  repulsion in semiconductor NCs was also considered in ref 26.

In the case for which  $\Delta_{xx}$  is positive and sufficiently large (compared with the transition line width), the excited-state absorption,  $\alpha_x$ , at the gain wavelength approaches zero and the gain threshold only depends on competition between stimulated emission and absorption arising from unexcited NCs. In this case, optical gain can, in principle, occur at  $N < 1$ ,<sup>24</sup> meaning that it can be realized in the *single-exciton* regime, for which Auger recombination is inactive. This result further suggests that the gain threshold should decrease as the localization regime changes from type I to type II (i.e., the  $x-x$  interaction energy switches from negative to positive).

Our experimental data indeed indicate the decrease in the gain threshold ( $N_{th}$ ) with decreasing wavelength during the transition from type I(S/S) to type II(S/C) regimes (Figure 4B, ●). Furthermore, the observed  $N_{th}$  minimum occurs roughly in the range of spectral energies corresponding to type II localization ( $\sim 500$  nm). Our estimations even indicate subunity magnitudes of  $N_{th}$ , which, however, requires additional verifications because of relatively large experimental uncertainties in the determination of the average NC populations in the case of hetero-NCs. Absolute excitation densities ( $N$ ) were estimated from analysis of the NC depopulation dynamics assuming that the fast ( $a_f$ ) and the slow ( $a_s$ ) components in the population decay are due to NCs occupied with multiexcitons and single excitons, respectively. We further assumed the Poisson statistics of NC populations, for which  $a_s \propto [1 - \exp(-N)]$  and  $a_f \propto [N - 1 + \exp(-N)]$ .

Overall, the above observations are consistent with the fact that, in addition to reduced Auger rates, type II localization facilitates achievement of the ASE regime because of reduced

excited-state absorption. This result further indicates the feasibility of a new approach to efficient NC-based lasing media via heterostructuring that favors the  $e-h$  charge separation and promotes repulsive  $x-x$  interactions. If these interactions are sufficiently strong, lasing can be realized in the single-exciton regime, for which Auger recombination is inactive. The elimination of Auger decay should lead to significantly extended optical gain lifetimes and, hence, dramatically reduced (by several orders of magnitude) lasing thresholds. Under these conditions, NC lasing can, in principle, be achieved using continuous-wave optical pumping or electrical injection.

**Acknowledgment.** We thank Dr. R. D. Schaller for helpful comments regarding the manuscript and Dr. D. Werder for transmission electron microscopy studies of synthesized materials. We also thank S. Sapra and Prof. D. D. Sarma of the India Institute of Science, Bangalore, India for X-ray photoemission measurements on the samples. This work was supported by Los Alamos LDRD Funds and the Chemical Sciences, Biosciences, and Geosciences Division of the Office of Basic Energy Sciences, Office of Science, U.S. Department of Energy.

**Supporting Information Available:** Synthesis, microstructural characterization, and theoretical models of ZnSe/CdSe inverted hetero-NCs. This material is available via the Internet at <http://pubs.acs.org>.

## References and Notes

- (1) Klimov, V. I.; Mikhailovsky, A. A.; Xu, S.; Malko, A.; Hollingsworth, J. A.; Leatherdale, C. A.; Eisler, H.-J.; Bawendi, M. G. *Science* **2000**, *290*, 314–317.
- (2) Klimov, V. I. Charge Carrier Dynamics and Optical Gain in Nanocrystal Quantum Dots: From Fundamental Photophysics to Quantum-Dot Lasing. In *Semiconductor and metal nanocrystals: synthesis and electronic and optical properties*; Klimov, V. I., Ed.; Marcel Dekker: New York, 2003, Chapter 5.
- (3) Mikhailovsky, A. A.; Malko, A. V.; Hollingsworth, J. A.; Bawendi, M. G.; Klimov, V. I. *Appl. Phys. Lett.* **2002**, *80*, 2380–2382.
- (4) Kazes, M.; Lewis, D. Y.; Ebenstein, Y.; Mokari, T.; Banin, U. *Adv. Mater.* **2002**, *14*, 317–321.
- (5) Schaller, R. D.; Petruska, M. A.; Klimov, V. I. *J. Phys. Chem. B* **2003**, *107*, 13765–13768.
- (6) Chepic, D. I.; Efros, A. L.; Ekimov, A. I.; Ivanov, M. G.; Kharchenko, V. A.; Kudriavtsev, I. A.; Yazeva, T. V. *J. Luminescence* **1990**, *47*, 113–127.
- (7) Klimov, V. I.; Mikhailovsky, A. A.; McBranch, D. W.; Leatherdale, C. A.; Bawendi, M. G. *Science* **2000**, *287*, 1011–1013.
- (8) Htoon, H.; Hollingsworth, J. A.; Dickerson, R.; Klimov, V. I. *Phys. Rev. Lett.* **2003**, *91*, 227401.
- (9) Hines, M. A.; Guyot-Sionnest, P. *J. Phys. Chem. B* **1996**, *100*, 468–471.
- (10) Dabbousi, B. O.; Rodriguez-Viejo, J.; Mikulec, F. V.; Heine, J. R.; Mattoussi, H.; Ober, R.; Jensen, K. F.; Bawendi, M. G. *J. Phys. Chem. B* **1997**, *101*, 9463–9745.
- (11) Reiss, P.; Bleuse, J.; Pron, A. *Nano Lett.* **2002**, *2*, 781–784.
- (12) Peng, X.; Schlamp, M. C.; Kadavanich, A. V.; Alivisatos, A. P. *J. Am. Chem. Soc.* **1997**, *119*, 7019–7029.
- (13) Cao, Y.-W.; Banin, U. *Angew. Chem., Int. Ed.* **1999**, *38*, 3692–3694.
- (14) Yongchi, Tian; Newton, T.; Kotov, N. A.; Guldi, D. M.; Fendler, J. H. *J. Phys. Chem.* **1996**, *100*, 8927–8939.
- (15) Kortan A. R.; Hull, R.; Opila, R. L.; Bawendi, M. G.; Steigerwald, M. L.; Carroll, P. J.; Brus, L. E. *J. Am. Chem. Soc.* **1990**, *112*, 1327–1332.
- (16) Zhou, H. S.; Honma, I.; Haus, J.-W.; Sasabe, H.; Komiyama, H. *J. Lumin.* **1996**, *70*, 21–34.
- (17) Mews, A.; Banin, U.; Kadavanich, A. V.; Alivisatos, A. P. *Ber. Bunsen (Phys. Chem. Chem. Phys.)* **1997**, *101*, 1621–1625.
- (18) Eychmüller, A.; Mews, A.; Weller, H. *Chem. Phys. Lett.* **1993**, *208*, 59–62.

(19) Braun, M.; Burda, C.; El-Sayed, M. A. *J. Phys. Chem. A* **2001**, *105*, 5548–5551.

(20) Battaglia, D.; Li, J. J.; Wang, Y. J.; Peng, X. G. *Angew. Chem., Int. Ed.* **2003**, *42*, 5035–5039.

(21) Kim, S.; Fisher, B.; Eisler, H.-J.; Bawendi, M. *J. Am. Chem. Soc.* **2003**, *125*, 11466–11467.

(22) Klimov, V. I.; Hunsche, S.; Kurz, H. *Phys. Rev. B* **1994**, *50*, 8110–8113.

(23) Kang, K. I.; Kepner, A. D.; Gaponenko, S. V.; Koch, S. W.; Hu, Y. Z.; Peyghambarian, N. *Phys. Rev. B* **1993**, *48*, 15449–15452.

(24) Achermann, M.; Hollingsworth, J. A.; Klimov, V. I. *Phys. Rev. B* **2003**, *68*, 245302.

(25) Butov, L. V.; Gossard, A. C.; Chemla, D. S. *Nature* **2002**, *418*, 751–754.

(26) Efros, Al. L.; Rodina, A. V. *Solid State Comm.* **1989**, *72*, 645.